Optimizing Dual-Axis Solar Panel Operation in an Agrivoltaic System and Implications for Power Systems

Anna Stuhlmacher
Michigan Technological University
annastu@mtu.edu

Johanna L. Mathieu
University of Michigan
jlmath@umich.edu

Peter Seiler
University of Michigan
pseiler@umich.edu

Abstract

The concept of agrivoltaics, or co-locating photovoltaic panels and crops, is viewed as a potential solution to competing land demands for food and energy production. In this paper, we propose an optimal dual-axis photovoltaic panel formulation that adjusts the panel position to maximize power generation subject to crop requirements. Through convex relaxations and shading factor approximations, we reformulate the problem as a convex second-order cone program and solve for the panel position adjustments away from the sun-tracking trajectory. We demonstrate our approach in a case study by comparing our approach with an approach that maximizes solar power capture and a scenario in which there are only crops. We found that we are able to successfully adjust the panel position while accounting for the trade-offs between the photovoltaic panels' energy production and the crop health. Additionally, optimizing the operation of an agrivoltaic system allows us to better understand agrivoltaic systems as a resource connected to the power grid.

Keywords: agrivoltaic systems, optimization, solar photovoltaics, food-energy nexus

1. Introduction

In a push to decarbonize energy systems, more renewable energy sources are being added to the electrical power grid. A challenge associated with installing renewable energy sources, such as solar photovoltaic (PV) panels, is limited land resources which are also needed for food production [1]. Agrivoltaics is considered as a potential approach to reduce the competing land use demands of energy and food production. Agrivoltaics is the concept of placing elevated PV panels over cropland. Initial studies have found that agrivoltaic systems can have a higher overall land use efficiency compared with just cropland or traditional ground-mounted PV installations (e.g., see [1] for details). Furthermore, co-locating crops and PV panels may have additional synergistic benefits, such as PV panel efficiency improving from evaporative cooling and a reduction in water irrigation needs due to crop shading. The performance of an agrivoltaic system is highly dependent on agricultural choices, PV system design and operation choices, and climate. As interest in agrivoltaic systems grows, it is important to better understand the potential impact of agrivoltaic systems on the power grid. Additionally, by characterizing an agrivoltaic system's performance, we can also evaluate the ability of agrivoltaic systems to actively participate in power systems operations, for example, by managing network constraints or providing ancillary services.

In this paper, we optimize the operation of dynamic PV panels within an agrivoltaic system to maximize value from both the PV system and the crops. Similar to traditional PV installations, PV panels within an agrivoltaic system experience variability in solar irradiance leading to intermittent and variable power generation. A large body of research has explored the impact of PV systems on the power grid as well as approaches to mitigate its negative effects, e.g., [2, 3]. Solar forecasting techniques help characterize the uncertainty present in PV systems. With this, we are better equipped to coordinate generation- and demand-side resources subject to distributed generation uncertainty [4, 5]. Unlike traditional PV installations, agrivoltaic systems are also dependent on the needs of the crops. Adjusting the PV system to ensure crop health impacts the agrivoltaic system's power generation variability. When accounting for trade-offs between the PV system and crops, agrivoltaic systems need to be treated as a different resource from traditional PV installations. Modeling and characterizing the optimal operation of agrivoltaic systems would allow us to better understand agrivoltaic systems as a resource that we can forecast and coordinate.

There is a growing body of research that examines the performance and implications of agrivoltaic systems. Existing literature evaluates and compares the benefits

and costs of agrivoltaic systems on a case-by-case basis. The performance of several different panel configurations and management choices are evaluated with models and simulations in [6] and [7]. In [8], the authors propose and simulate tracking schemes for single-axis bifacial panels while considering the desired effective photosynthetically active radiation for crops. An experimental testbed is developed in [9] that measures an agrivoltaic system's food production, environmental impacts, and power production for different agricultural species. While these works provide valuable insight into the benefits and trade-offs in agrivoltaic systems, formal optimization approaches are important tools for determining the best design and operation choices. Very few papers develop optimization formulations for agrivoltaic system design or operation, with exception of [10], which employs a genetic algorithm to solve for the PV design parameters (i.e., azimuth angle and row distance) of static bifacial vertically mounted panels subject to crop and PV system modeling. To the best of our knowledge, there are no papers that explicitly optimize the real-time operation of dynamic PV panels.

To address this, we formulate the operation of dual-axis solar PV panels as an optimization problem subject to the PV system and crop constraints. A challenge associated with this problem is incorporating the different timescales of the crop and PV outcomes. To capture the power generation and crop growth time scales, we separate the optimal agrivoltaic operation problem into two subproblems – a months-long problem that considers the growing season crop yield goals and a daily PV operational problem that adjusts the PV panels based on PV power output and crop health goals. In this work, we formulate the daily dual-axis PV operation problem that solves for the PV panel adjustments that maximize power output while meeting crop needs. The problem can be updated over the optimization horizon given improved forecasting and measurements. The contributions of this paper are i) presenting a framework to co-optimize the crop yield and PV power output as two subproblems, ii) formulating an optimal dual-axis PV operation problem that captures the PV power generation, panel shading on the crops, and crop health constraints, iii) evaluating the relationship between PV panel position and crop shading, iv) reformulating the problem into a convex program given trigonometric properties and shading factor approximations, and v) demonstrating the performance of our approach in a case study.

The rest of the paper is organized as follows. In Section 2, we discuss the full problem and the separation of time scales. Section 3 formulates the daily operational problem and Section 4 reformulates the problem as a convex second order cone program (SOCP). We demonstrate our approach in Section 5 and concluding remarks are provided in Section 6.

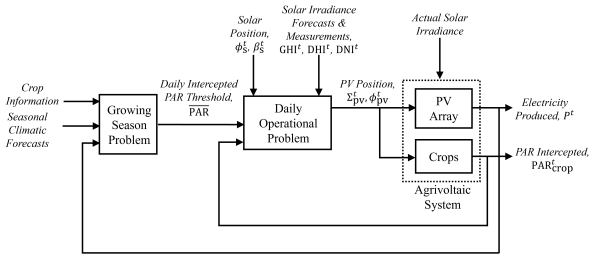

Figure 1. Block diagram of the approach to manage an agrivoltaic system's long- and short- term goals.

2. Problem overview

We consider an agrivoltaic system with dual-axis PV panels over crops. Agrivoltaic systems that use dual- or single-axis PV panels have several potential advantages compared to static, or fixed, PV panels: the PV panels can be adjusted throughout the day to i) significantly increase power generation or ii) allow more sunlight to reach the crops below. While we consider dual-axis panels in this paper, the formulation can also simplify to single-axis PV systems. Within an agrivoltaic system, we need to consider the states and outcomes of both the crops and the PV system. The timescales for PV power production and crop growth are drastically different. For instance, PV power output is dependent on the solar irradiance which varies on the seconds timescale. Crops, on the other hand, are robust at short time scales. The health and yield of crops are typically considered over entire growing seasons subject to the daily intercepted photosynthetically active radiation (PAR), which is the range of solar radiation wavelengths that is useful for plant photosynthesis.

We separate this problem into two subproblems to capture the timescales of the crop needs and PV power output. Fig. 1 illustrates this separation with a block diagram, where the slower outer loop is the growing season problem and the faster inner loop is the daily PV operational problem. The growing season problem captures the longer-scale outcomes, i.e., the crop growth and yield over the entire growing season. This problem incorporates the crop models to estimate biomass, yield, and economic value given climatic forecasts as well as water and fertilizer applications. This problem determines the minimum daily intercepted PAR, $\overline{\text{PAR}}$, for the crops in the daily PV operational problem as a proxy for crop health. The PAR received by the crops

can be used to determine crop yield [10]. The seasonal problem can be updated throughout the growing season given climatic uncertainty realizations (e.g., irradiance, precipitation, and temperature), observed PV panel energy generation, and crop/soil health measurements. In the daily operational problem, we adjust the dual-axis PV panels away from the sun-tracking algorithm (i.e., panel positions to maximize power output from direct beam irradiance) in order to ensure that the crops receive the required amount of daily PAR to meet season-long crop health/yield goals. The daily PV operational problem can be updated through the day given the PAR realizations. In this work, we focus on the daily PV operational problem. In future work, we plan to implement the growing season problem.

3. Daily operational formulation

In this section, we present the daily operational problem. We solve for the PV panel adjustments away from the sun-tracking position to meet the requirement for the daily PAR intercepted by the crops, $\overline{\text{PAR}}$, which is determined within the growing season problem. We solve the problem for a 24-hour horizon with T time steps of duration ΔT, i.e., $t = 1, ..., T$ where $T \cdot \Delta T = 24$ h. The daily operational problem can be updated throughout the day given uncertainty realizations and improved forecasting. The inner loop in Fig. 1 illustrates the daily operational problem. In the following subsections, the model inputs, variables, and constraints are defined.

3.1. Inputs

The daily operational problem is dependent upon the solar position and irradiance. Solar position–which is location and time specific–is used for solar tracking and crop shading calculations. The solar position at time period t within the daily optimization horizon can be described by the solar azimuth angle ϕ_{s}^t (i.e., the angle between the sun and true south) and the solar altitude angle β_{s}^t (i.e., the angle between the sun and the local horizon). These solar position inputs are illustrated in the left diagram of Fig. 2. Electricity production and crop growth are dependent on solar irradiance. Solar irradiance can be decomposed into direct beam, diffuse, and reflective components. The diffuse component is particularly important to account for with partially shaded crops (i.e., agrivoltaic systems) [11]. As a result, we consider the direct beam and diffuse components of the solar irradiance, I_{db}^t and I_{diff}^t, respectively. In our case study, we use measurements of the Global Horizontal Irradiance (GHI), Direct Normal Irradiance (DNI), and Diffuse Horizontal Irradiance (DHI) to determine the irradiance on the PV collectors and the PAR received by the crops at a specific location and time step. The total PAR available, $\text{PAR}_{\text{total}}^t$, can be estimated from the GHI at time t

$$\text{PAR}_{\text{total}}^t = \alpha \text{GHI}^t, \tag{1}$$

where α is the PAR-GHI ratio.

We calculate the power generated by the PV panels given the irradiance and panel position in Section 3.2 and the PAR that reaches the crops in Section 3.4, taking into account the crop shading in Section 3.3.

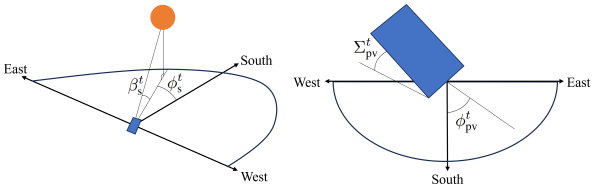

Figure 2. (Left) Solar position can be described by the solar azimuth angle ϕ_{s}^t and the solar altitude angle β_{s}^t. (Right) PV panel position can be described by the panel's azimuth angle ϕ_{pv}^t and the panel's tilt angle Σ_{pv}^t.

3.2. PV power output

For dual-axis solar PV panels, we can describe a PV panel's position at each time step t in terms of two degrees of freedom: the PV panel's azimuth angle ϕ_{pv}^t (i.e., the angle between the normal of the PV panel's surface and true south, where east of south is positive) and tilt Σ_{pv}^t (i.e., the angle between the PV collector surface and horizontal). These PV panel position variables are illustrated in the right diagram of Fig. 2. We assume that all panels within an agrivoltaic system follow the same position controls since it is common for PV panels within an installation to be controlled the same way; however, notation can easily be added to the formulation to allow for independent position choices for each panel. The range of PV panel positions is bounded by the PV system design

$$\underline{\phi}_{\text{pv}} \leq \phi_{\text{pv}}^t \leq \overline{\phi}_{\text{pv}}, \tag{2}$$

$$\underline{\Sigma}_{\text{pv}} \leq \Sigma_{\text{pv}}^t \leq \overline{\Sigma}_{\text{pv}}, \tag{3}$$

where $\underline{\phi}_{\text{pv}}$ and $\overline{\phi}_{\text{pv}}$ are the minimum and maximum azimuth angle and $\underline{\Sigma}_{\text{pv}}$ and $\overline{\Sigma}_{\text{pv}}$ are the minimum and maximum tilt angle.

When considering the PV power output, it is important to define the incidence angle $\theta_{\text{s-pv}}^t$, or the angle between the sun's rays and the normal vector of the

PV panel's surface. The relation between $\theta^t_{\text{s-pv}}$ and the position of the sun and PV panel at time t is

$$\cos\theta^t_{\text{s-pv}} = \cos\beta^t_{\text{s}}\cos\left(\phi^t_{\text{s}} - \phi^t_{\text{pv}}\right)\sin\Sigma^t_{\text{pv}} + \sin\beta^t_{\text{s}}\cos\Sigma^t_{\text{pv}}. \quad (4)$$

Given the DNI and DHI, we can calculate the direct beam irradiance I^t_{db} and diffuse irradiance I^t_{diff} on the PV collector at time t [12]

$$I^t_{\text{db}} = \text{DNI}^t \cdot \cos\theta^t_{\text{s-pv}}, \quad (5)$$

$$I^t_{\text{diff}} = \text{DHI}^t \cdot \left(\frac{1+\cos\Sigma^t_{\text{pv}}}{2}\right). \quad (6)$$

The power production P^t of the PV system at time t is

$$P^t = A_{\text{array}} \cdot \eta_{\text{array}} \cdot \left(I^t_{\text{db}} + I^t_{\text{diff}}\right), \quad (7)$$

where A_{array} is the net surface area of the PV array and the efficiency η_{array} of the PV array is dependent on the ambient air temperature, wind speed, dust accumulation, and PV material. The PV efficiency is generally around 15-23%. Note that this equation does not consider shading between panels given that the PV panels within agrivoltaic systems are typically set up in a less dense configuration than traditional PV installations. In this formulation, we neglect the impact of reflected irradiance on the PV panels and crops since the contribution of reflected irradiance on monofacial panels can be very modest [13].

In our formulation, we assume that the dual-axis PV system tracks the sun's position and that adjustments are made from this trajectory to meet the crop PAR needs. A simple sun-tracking (ST) strategy maximizes the direct beam irradiance (i.e., $\theta^t_{\text{pv-s}} = 0$)

$$\Sigma^t_{\text{pv, st}} = 90^\circ - \beta^t_{\text{s}}, \quad (8)$$

$$\phi^t_{\text{pv, st}} = \phi^t_{\text{s}}, \quad (9)$$

where $\Sigma^t_{\text{pv, st}}$ and $\phi^t_{\text{pv, st}}$ are the PV tilt and azimuth position at time t when following the sun-tracking trajectory. To make adjustments from the sun-tracking trajectory, we define the PV panel positions as

$$\Sigma^t_{\text{pv}} = \delta\Sigma^t_{\text{pv}} + \Sigma^t_{\text{pv, st}}, \quad (10)$$

$$\phi^t_{\text{pv}} = \delta\phi^t_{\text{pv}} + \phi^t_{\text{pv, st}}, \quad (11)$$

where $\delta\Sigma^t_{\text{pv}}$ and $\delta\phi^t_{\text{pv}}$ are the PV tilt and azimuth angle adjustments away from the sun-tracking position. Given the irradiance and power definitions (5)-(7) and the PV panel position definitions (10)-(11), we can write the PV irradiance deviations δI^t_{db} and δI^t_{diff} and the power output deviation δP^t away from the sun-tracking algorithm (8)-(9) at time t as

$$\delta I^t_{\text{db}} = \text{DNI}^t \cdot \left(\cos\left(\theta^t_{\text{s-pv}}\right) - 1\right), \quad (12)$$

$$\delta I^t_{\text{diff}} = \text{DHI}^t \cdot \left(\frac{\cos\left(\Sigma^t_{\text{pv}}\right) - \cos\left(\Sigma^t_{\text{pv,st}}\right)}{2}\right), \quad (13)$$

$$\delta P^t = A_{\text{array}} \cdot \eta_{\text{array}} \cdot \left(\delta I^t_{\text{db}} + \delta I^t_{\text{diff}}\right). \quad (14)$$

3.3. Shading analysis

A shading factor function is used to determine the amount of PAR that reaches the crops at time t, similar to [10]

$$\text{PAR}^t_{\text{crop}} = \left(1 - S_F(\delta\phi^t_{\text{pv}}, \delta\Sigma^t_{\text{pv}})\right) \cdot \text{PAR}^t_{\text{total}}, \quad (15)$$

where shading factor function $S_F(\cdot)$ is dependent on the PV panel and solar positions. The shading factor is the percent of the field that is shaded given the solar and PV position and is calculated using the geometric shading calculation procedure in [14]. Note that we can extend this process to define the shading factor at a smaller spatial resolution, e.g., if we want to examine the impact of edge and interrow shading.

3.4. Crop model

The crops' photosynthesis rate can be modeled with light response curves [11,15], where there is a minimum required PAR level for photosynthesis (i.e., the light compensation point). The photosynthesis rate increases almost linearly with increases in PAR until reaching a PAR level associated with the maximum photosynthesis rate (i.e., the light saturation point). After the light saturation point, the rate of photosynthesis levels out and then actually decreases (i.e., photoinhibition). Plants that are considered shade tolerant have lower light saturation points. In this work, we consider PAR in terms of photosynthetic radiant flux density, with units of W/m^2.

In our problem, we enforce a lower bound on the daily intercepted PAR for the crops

$$\sum_{t=1}^{T} \text{PAR}^t_{\text{crop}} \cdot \Delta T \geq \overline{\text{PAR}}, \quad (16)$$

where $\overline{\text{PAR}}$ is the minimum daily intercepted PAR threshold, $\text{PAR}^t_{\text{crop}}$ is the PAR received by the crops at time t, and ΔT is the duration of the time step. The PAR target threshold is determined within the

seasonal operational planning problem, incorporating crop information and forecasts for the entire growing season. The daily intercepted PAR is used in crop models to determine the biomass production, crop yield, and economic yield. For instance, the daily intercepted PAR is an input in the EPIC crop model [16].

4. Optimal PV operation framework

We can then write the daily PV operational problem for the dual-axis PV panels over the crops as

$$\max_{\mathbf{x}} \quad \sum_{t=1}^{T} \pi^t \cdot \delta P^t \cdot \Delta T \qquad \text{(P1)}$$

$$\text{s.t.} \quad (2)-(4), (8)-(16) \quad \forall\, t = 1...T,$$

where π^t is the price of electricity produced. In (P1), we solve for the PV panel adjustments away from the sun-tracking position subject to the PAR requirements, shading analysis, and PV power generation constraints over the optimization horizon. We want to maximize the total value of energy produced relative to the sun-tracking position. The decision variables in $\mathbf{x}$ are δI^t_{db}, δI^t_{diff}, δP^t, $\delta\phi^t_{\text{pv}}$, $\delta\Sigma^t_{\text{pv}}$, ϕ^t_{pv}, Σ^t_{pv}, $\theta^t_{\text{s-pv}}$, and $\text{PAR}^t_{\text{crop}}$. We solve for the PV panel operation over the entire optimization horizon and can re-solve the problem for the remaining horizon (i.e., $t = t_k...T$) given updated irradiance forecasts and measurements.

The optimization formulation (P1) is nonconvex due to the incidence angle (4), irradiance deviations (12)-(13), and shading factor function in (15). Since nonconvex problem can be hard to solve, we use variable redefinitions, convex relaxations, and a shading factor function approximation to reformulate the problem as a convex problem. We describe our approach in the following subsections and analyze its performance in the original, nonconvex constraints in Section 5.3.

4.1. Shading factor function approximation

We first evaluate the relationship between the shading factor and the PV panel position. We simulate the shading pattern and the impact of adjusting the tilt and azimuth away from the sun-tracking position. Specifically, one degree of freedom (i.e., PV azimuth or tilt) of the PV panel is fixed while the other is adjusted. The shading factor difference from the sun-tracking algorithm is calculated for the full range of angle adjustments (while still within the angle limits) with a resolution of 1°. With our case study presented in Section 5, we simulate the shading factor over the full range of feasible angle adjustments at each 10-minute time step over the 24-hour horizon.

We observe that varying the azimuth has no clear impact on the shading factor. This is because we are rotating the panel around the z-axis. For instance, consider the case where the panels have a tilt of zero. When the azimuth is adjusted, the only changes to the shading factor are due to the shadows being projected outside the field perimeter. Consequently, in our formulation, we do not adjust the PV panel azimuth away from the sun-tracking algorithm.

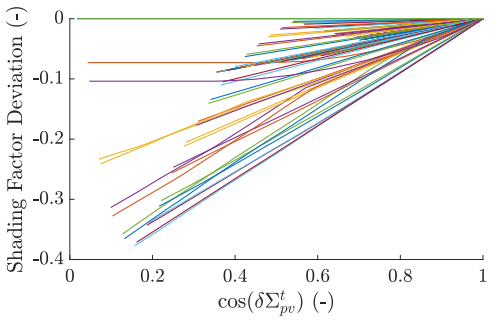

Figure 3. Shading factor deviations given the cosine of the tilt angle adjustments away from the sun-tracking algorithm. Resolution of 1° steps where each line is a 10-minute time step within the optimization horizon. At each time step, the full range of feasible tilt angle adjustments were considered, i.e., $\Sigma^t_{\text{pv}} \in [\Sigma^t_{\text{pv,st}} \pm 90^\circ$ s.t. (3)].

Alternatively, we observed that the tilt adjustments away from the sun-tracking algorithm always reduce the shading factor. In Fig. 3, we observed that the difference in the shading factor from the sun-tracking algorithm at every time step t has a strong linear relationship with the cosine of the tilt angle adjustment, $\cos(\delta\phi^t_{\text{pv}})$. As a result, we fit a linear function at time t to determine the shading factor given the tilt angle adjustments, i.e.,

$$S^t_{\text{F}} = g^t_1 \cdot \cos\left(\delta\Sigma^t_{\text{pv}}\right) + g^t_2, \qquad (17)$$

where g^t_1 and g^t_2 are parameters of the linearization. We found that the residuals between the estimated linear function and the actual shading factor deviations were small, generally less than 10^{-4}. Fig. 4 shows the R^2 values of the best fit linear approximation. It should be noted that the R^2 value is one for all time periods except for those within the first and last 40 minutes of daylight hours. The R^2 values less than one are most likely due to the low solar altitude (less than 9°) when the sun rises and sets. The shadows cast are usually outside of the crop field borders for a range of angles, leading to flattened parts of the curve. However, the accuracy of the linear approximation may be less significant at these time periods since the sunlight intensity is less than

during peak daylight hours and it only affects a small range of time steps. In future work, we will investigate how we can approximate the shading factor deviations as a multivariable function that also includes the time of day (i.e., based on solar position and site location).

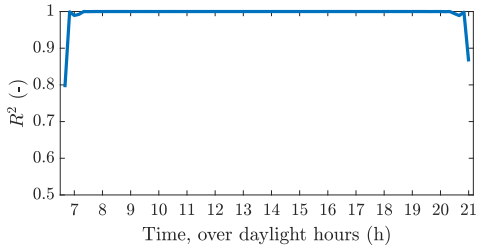

Figure 4. R^2 values of the linear approximations over the daylight hours in the case study.

4.2. Variable redefinitions

We define variables

$$x^t := \cos(\delta\Sigma^t_{\text{pv}}), \quad y^t := \sin(\delta\Sigma^t_{\text{pv}}),$$

and use sine and cosine properties, i.e.,

$$\sin(x+y) = \sin(x)\cos(y) + \cos(x)\sin(y),$$
$$\cos(x+y) = \cos(x)\cos(y) - \sin(x)\sin(y),$$

to rewrite the nonconvex constraints as linear functions of x^t and y^t. Specifically, we can write the irradiance deviations (12)-(13), the PAR received by the crops (15), and the PV tilt angle limits (3) as

$$\delta I^t_{\text{db}} = a^t_1 x^t + a^t_2, \tag{18}$$
$$\delta I^t_{\text{diff}} = b^t_1 x^t + b^t_2 y^t + b^t_3, \tag{19}$$
$$\text{PAR}^t_{\text{crop}} = c^t_1 x^t + c^t_2, \tag{20}$$
$$0 \le d^t_1 x^t + d^t_2 y^t \le 1, \tag{21}$$

where parameters a^t_1, a^t_2, b^t_1, b^t_2, b^t_3, c^t_1, c^t_2, d^t_1, and d^t_2 are dependent on the solar irradiance and position

$$a^t_1 := \text{DNI}^t,$$
$$a^t_2 := \text{-DNI}^t,$$
$$b^t_1 := \frac{1}{2}\text{DHI}^t \cos(90^\circ - \beta^t_{\text{s}}),$$
$$b^t_2 := \text{-}\frac{1}{2}\text{DHI}^t \sin(90^\circ - \beta^t_{\text{s}}),$$
$$b^t_3 := \text{-}\frac{1}{2}\text{DHI}^t \cos(90^\circ - \beta^t_{\text{s}}),$$
$$c^t_1 := \text{-}g^t_1 \cdot \text{GHI}^t \alpha,$$
$$c^t_2 := \alpha\text{GHI}^t - g^t_2 \cdot \alpha\text{GHI}^t,$$
$$d^t_1 := \sin(90^\circ - \beta^t_{\text{s}}),$$
$$d^t_2 := \cos(90^\circ - \beta^t_{\text{s}}).$$

In the appendix, we outline our derivation.

When we replace $\cos\delta\Sigma^t_{\text{pv}}$ and $\sin\delta\Sigma^t_{\text{pv}}$ with x^t and y^t, we need to ensure that

$$(x^t)^2 + (y^t)^2 = 1, \tag{22}$$

in order to recover a single $\delta\Sigma^t_{\text{PV}}$ value. We replace (22) with the second order cone relaxation

$$(x^t)^2 + (y^t)^2 \le 1, \tag{23}$$

and evaluate the exactness of the convex relaxation in Section 5.3.

4.3. Convex reformulation

Using the approximations and relaxations in Sections 4.1-4.2, we reformulate the optimization problem (P1) as a convex second order cone program

$$\max_{\mathbf{x}} \quad \sum_{t=1}^{T} \pi^t \cdot \delta P^t \cdot \Delta T \tag{P2}$$
$$\text{s.t.} \quad (14), (16), (18)-(21), (23) \quad \forall\, t = 1...T.$$

The decision variables in $\mathbf{x}$ are x^t, y^t, δI^t_{db}, δI^t_{diff}, δP^t, and $\text{PAR}^t_{\text{crop}}$. If (22) is true given the optimal x^t and y^t, (23) is exact and we can recover $\delta\Sigma^t_{\text{pv}}$ by solving $\delta\Sigma_{\text{pv}} = \sin^{-1}(y^t)$. Otherwise, we recover a more conservative tilt deviation by determining maximum magnitude tilt deviation from x^t and y^t separately. This causes $\delta\Sigma^t_{\text{pv}}$ to be higher than necessary, leading to potentially more PAR received by the crops and less PV power output. This is discussed further in Section 5.3.

5. Case study

In our case study, we evaluate our approach on a synthetic agrivoltaic system.

5.1. Set up

We consider the performance of a synthetic agrivoltaic system located at the University of Michigan's Campus Farm in Ann Arbor, Michigan (42.3°N, 83.7°W). The PV system has 7 rows, with 20 pairs of PV panels per row. We draw PV panel specifications from Heliene's 132HC M10 TPC SL Monofacial Module with an estimated efficiency of

$\eta_{\text{array}} = 22\%$ [17]. The rows are separated by 6 meters, the intrarow PV pair spacing is 2.5 meters, and the center of each PV panel pair is elevated 4.5 meters above the ground (see Fig. 5 for reference). The overall ratio of PV panel surface area to crop field surface area is approximately 13%, similar to existing agrivoltaic installations [18].

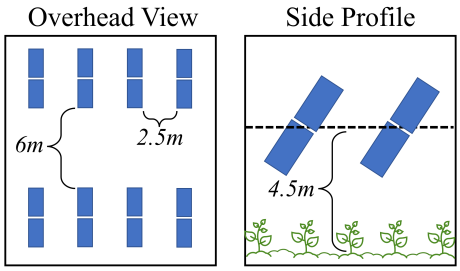

Figure 5. Example overhead (left) and side (right) views of the agrivoltaic system configuration. The blue shapes represent the individual PV panels. The graphics show a portion of the agrivoltaic system for illustrative purposes.

We evaluate our formulation with historical solar irradiance data. We pull GHI^t, DHI^t, and DNI^t values from the National Solar Radiation Database (NSRDB) [19]. We consider a 24-hour time horizon, pulling the NSRDB data from July 14, 2021 with a time resolution of 30 minutes. The solar azimuth angle ϕ_{s}^t and altitude angle β_{s}^t are calculated with the solar position algorithm in the Python package pvlib [20], with a time resolution of 10 minutes. We set $\Delta T = 1/6$ h and update the PV panel position every 10 minutes. As a result, $T = 144$.

We consider several different $\overline{\text{PAR}}$ thresholds that are dependent upon the light saturation point (LSP)

$$\overline{\text{PAR}} = c \cdot \text{LSP} \cdot \Delta T_{\text{daylight}}, \tag{24}$$

where c is a fraction that we vary and $\Delta T_{\text{daylight}}$ are the number of daylight hours within the optimization horizon. We use the LSP of lettuce for the purpose of this case study.

The electricity prices π^t are shown in Fig. 6. Additional parameters are shown in Table 1. We solve (P2) with the Gurobi solver [21] using the JuMP package in Julia. The code and test case are publicly available on GitHub [22].

5.2. Illustrative results

We first solve the reformulated optimization problem (P2) presented in Section 4.3. We consider different $\overline{\text{PAR}}$ values by varying c in (24). Table 2 compares the daily PAR intercepted by the crops and the PV energy output for three cases: (P2) for four c values, a case where the PV panels follow the sun-tracking algorithm (i.e., (8)-(9)), and a conventional crop-only case (i.e., there is no overhead PV system). It should be noted that the daily crop PAR values in the (P2) solutions are equal to their respective required minimum PAR threshold. To meet $\overline{\text{PAR}}$, the PV panels in the (P2) solutions generate less energy than in the sun-tracking case. This indicates that the daily optimization problem adjusts the PV panels away from the sun-tracking position to meet crop PAR needs. For example, there is a 0.7% to 46.1% reduction in PV energy output given the choice in c. As c increases, the $\overline{\text{PAR}}$ increases, requiring the PV panels to move further away from the sun-tracking position in order to let more sunlight through to the crops. As a result, we see a reduction in the energy output from the panels and an increase in the cumulative crop PAR. This illustrates the trade-offs between the PAR received by the crops and the energy produced by the PV system and provides motivation for formulating the growing season problem that can capture and maximize the overall value of these systems in terms of the energy produced and seasonal crop yield.

Furthermore, Table 2 demonstrates that we can characterize the energy output from the agrivoltaic system given different crop needs. By being able to reliably forecast the time-varying power output within an agrivoltaic system, we are better positioned to coordinate agrivoltaic systems to support power systems operations. It should be noted that the agrivoltaic

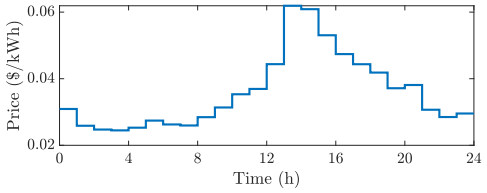

Figure 6. Time-varying electricity price over the optimization horizon.

Table 1. Case Study Parameters

Parameters	Values
α	0.44
A_{array}	667.4 m^2
$\underline{\Sigma}_{\text{pv}}, \overline{\Sigma}_{\text{pv}}$	$0°, 90°$
$\underline{\phi}_{\text{pv}}, \overline{\phi}_{\text{pv}}$	$-180°, 180°$
$\Delta T_{\text{daylight}}$	14.3 h
LSP of Lettuce [8]	213 W/m^2
Field Dimensions	72.7 m $\times$ 71.4 m
PV Pair Dimensions	1.135 m $\times$ 4.2 m

system design and configuration will have a significant impact on the PV power output and crop performance, underscoring the importance of this consideration within any cost-benefit analysis.

Table 2. Intercepted daily crop PAR and PV energy output for the crop only case, the sun tracking algorithm, and the proposed optimization at varying c values within the $\overline{\text{PAR}}$ threshold.

Approach	PAR ($\text{Wh}/\text{m}^2/\text{d}$)	Energy (kWh)
Crop Only	2847.5	0
Sun Tracking (ST)	2413.4	1137.3
(P2), $c = 80\%$	2443.5	1129.6
(P2), $c = 82\%$	2504.6	1020.5
(P2), $c = 85\%$	2596.3	816.7
(P2), $c = 88\%$	2687.9	613.1

5.3. Analysis of computational performance

We next evaluate the exactness of the convex relaxation (23) on our solution. We found that the relaxation is not always exact for all time periods and c values. The one exception is $c = 80\%$, where the relaxation is always exact. For the higher values of c, we found that x^t and y^t were zero when (22) did not hold. Given our strategy of choosing the largest magnitude $\delta\Sigma^t_{\text{pv}}$ from x^t and y^t, this yields $\delta\Sigma^t_{\text{pv}} = 90°$, which adjusts the panel's surface to be perpendicular to the sun's rays and lets the maximum amount of light through to the crops. In this case, the actual crop PAR would be higher than what is estimated in the optimization problem (e.g., at $c = 85\%$, the actual daily intercepted crop PAR was 2597.3 $\text{Wh}/\text{m}^2/\text{d}$ compared to (P2)'s estimated 2596.3 $\text{Wh}/\text{m}^2/\text{d}$). However, these large tilt angle deviations lead to Σ^t_{pv} values outside of the physical range we chose in our case study, i.e., $0 \leq \Sigma^t_{\text{pv}} \leq 90°$. When we force the tilt angle to be within its limits, the PAR is then underestimated (e.g., the actual daily intercepted PAR for $c = 85\%$ with its tilt limits enforced is 2502 $\text{Wh}/\text{m}^2/\text{d}$). It should be noted that if the PV panels had a tilt range of $(-90°, 90°)$ then we would be capable of making this $90°$ adjustment. This indicates that PV panel configuration and tilt limits impact the constraint relaxation performance.

Last, we investigate the shading factor approximation performance within the original problem (P1). In order to only consider the impact of the shading factor approximation, we examine the case where the relaxation is exact, i.e., $c = 80\%$. Given the optimal PV positions from (P2), we simulate the shading factor and PAR received by the crops given the original geometric shading factor calculations discussed

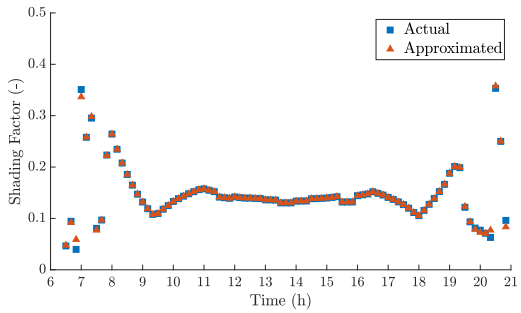

Figure 7. Actual (blue square) and approximated (red triangle) shading factor S_{F} over the optimization horizon for $c = 80\%$ given the Σ^t_{pv} calculated from the (P2) solution.

in Section 3.3. Fig. 7 plots the actual and approximated shading factors given the PV panel position choices from (P2). We can observe that the shading factor approximation is very close to the actual shading factor, where the performance is slightly worse in the first and last daylight hours. This is to be expected given the higher R^2 values during the first and last hour in Fig. 4. We found that the average percent difference between the actual and approximated shading factor was 0.49%. Furthermore, as we noted in Section 4.1, since there is less sunlight in the morning and evening hours compared with midday, when we factor in the irradiance magnitudes, the errors in the shading factor approximation is less significant in the first and last hours. For instance, when $c = 80\%$, the actual and approximated daily crop PARs are nearly identical, with a percent difference of 0.002%.

6. Conclusion

In this paper, we investigated the optimal operation of an agrivoltaic system. The motivation for this work is being better able to understand agrivoltaic systems as a distributed generation resource and its implications for the power grid. We proposed an approach to optimize the value of the crops and PV system within an agrivoltaic system. To capture the different timescales of this problem, we separate the problem into two subproblems and we focus on the fast daily PV operational problem. We formulated the daily operational PV problem that determines the dual-axis PV panel position to meet crop PAR thresholds (as a proxy for crop health) subject to crop shading while maximizing the power generated by the PV panels. Using shading factor approximations and convex relaxations, we are able to reformulate the problem as a SOCP. We solve for the PV tilt angle

deviation away from the sun-tracking algorithm.

Through a case study, we are able to demonstrate that the daily optimization problem can successfully adjust the PV panels away from the sun-tracking position to meet crop PAR needs. Additionally, we found that the shading factor approximation performs well. However, the convex relaxation was not always exact, leading to overestimates of the daily intercepted crop PAR. Future work will explore incorporating the growing season problem and updating the solution as a model predictive control formulation with a rolling horizon to manage irradiance uncertainty and quantifying the impact on power systems operation.

A. Appendix

We summarize the derivation of the linear constraints (18)-(21).

Irradiance Deviations: For the direct beam irradiance deviation, we plug (4) and (8)-(11) into (12). Given $\delta\phi^t_{\text{pv}} = 0$, we use the sine property to simplify the incidence angle terms to x^t, resulting in

$$\delta I^t_{\text{db}} = \text{DNI}^t x^t - \text{DNI}^t.$$

For the diffuse irradiance deviation, we plug (8) and (10) into (13). We expand out the $\cos(90^\circ - \beta^t_{\text{s}} + \delta\Sigma^t_{\text{pv}})$ term using the cosine property to get

$$\delta I^t_{\text{diff}} = \frac{1}{2}\text{DHI}^t \cdot \big(\cos(90^\circ - \beta^t_{\text{s}}) \cdot x^t - \sin(90^\circ - \beta^t_{\text{s}}) \cdot y^t - \cos(90^\circ - \beta^t_{\text{s}}) \big).$$

PAR crop: For the PAR received by the crops, we plug (1) and (17) into (15) to get

$$\text{PAR}^t_{\text{crop}} = \alpha \text{GHI}^t \cdot \left(-g^t_1 x^t - g^t_2 + 1 \right).$$

Tilt Limits: For the PV tilt angle limits, we plug (8) and (10) into (3). Since the sine function is increasing over the feasible values of Σ^t_{pv} and the sine function is odd, we take the sine function of all sides of the inequality and use the sine property to expand the $\sin(90^\circ - \beta^t_{\text{s}} + \delta\Sigma^t_{\text{pv}})$ term, yielding

$$0 \leq \sin(90^\circ - \beta^t_{\text{s}}) \cdot x^t + \cos(90^\circ - \beta^t_{\text{s}}) \cdot y^t \leq 1.$$

References

[1] J. Macknick, H. Hartmann, G. Barron-Gafford, B. Beatty, R. Burton, C. Seok-Choi, M. Davis, R. Davis, J. Figueroa, A. Garrett, L. Hain, S. Herbert, J. Janski, A. Kinzer, A. Knapp, M. Lehan, J. Losey, J. Marley, J. MacDonald, J. McCall, L. Nebert, S. Ravi, J. Schmidt, B. Staie, and L. Walston, "The 5 Cs of agrivoltaic success factors in the United States: Lessons from the InSPIRE research study," National Renewable Energy Lab. (NREL), Golden, CO (United States), Tech. Rep. NREL/TP-6A20-83566, 2022.

[2] S. Eftekharnejad, V. Vittal, G. T. Heydt, B. Keel, and J. Loehr, "Impact of increased penetration of photovoltaic generation on power systems," *IEEE Transactions on Power Systems*, vol. 28, no. 2, pp. 893–901, 2013.

[3] M. M. Begovic, I. Kim, D. Novosel, J. R. Aguero, and A. Rohatgi, "Integration of photovoltaic distributed generation in the power distribution grid," in *45th Hawaii International Conference on System Sciences (HICSS)*. IEEE, 2012, pp. 1977–1986.

[4] J. Liu, M. G. Martinez, B. Li, J. Mathieu, and C. L. Anderson, "A comparison of robust and probabilistic reliability for systems with renewables and responsive demand," in *49th Hawaii International Conference on System Sciences (HICSS)*, 2016, pp. 2373–2380.

[5] Z. Wang and C. L. Anderson, "A progressive period optimal power flow for systems with high penetration of variable renewable energy sources," *Energies*, vol. 14, no. 10, 2021.

[6] S. Amaducci, X. Yin, and M. Colauzzi, "Agrivoltaic systems to optimise land use for electric energy production," *Applied Energy*, vol. 220, pp. 545–561, 2018.

[7] C. Dupraz, H. Marrou, G. Talbot, L. Dufour, A. Nogier, and Y. Ferard, "Combining solar photovoltaic panels and food crops for optimising land use: Towards new agrivoltaic schemes," *Renewable Energy*, vol. 36, no. 10, pp. 2725–2732, 2011.

[8] H. Imran, M. H. Riaz, and N. Z. Butt, "Optimization of single-axis tracking of photovoltaic modules for agrivoltaic systems," in *47th Photovoltaic Specialists Conference (PVSC)*. IEEE, 2020, pp. 1353–1356.

[9] G. A. Barron-Gafford, M. A. Pavao-Zuckerman, R. L. Minor, L. F. Sutter, I. Barnett-Moreno, D. T. Blackett, M. Thompson, K. Dimond, A. K. Gerlak, G. P. Nabhan, and J. E. Macknick, "Agrivoltaics provide mutual benefits across the food–energy–water nexus in drylands," *Nature Sustainability*, vol. 2, no. 9, pp. 848–855, 2019.

[10] P. E. Campana, B. Stridh, S. Amaducci, and M. Colauzzi, "Optimisation of vertically mounted agrivoltaic systems," *Journal of Cleaner Production*, vol. 325, p. 129091, 2021.

[11] S. Ma Lu, S. Zainali, B. Stridh, A. Avelin, S. Amaducci, M. Colauzzi, and P. Campana, "Photosynthetically active radiation decomposition models for agrivoltaic systems applications," *Solar Energy*, vol. 244, pp. 536–549, 2022.

[12] G. M. Masters, *Renewable and efficient electric power systems*. John Wiley & Sons, 2013.

[13] J. S. Pulido-Mancebo, R. López-Luque, L. M. Fernández-Ahumada, J. C. Ramírez-Faz, F. J.

Gómez-Uceda, and M. Varo-Martínez, "Spatial distribution model of solar radiation for agrivoltaic land use in fixed PV plants," *Agronomy*, vol. 12, no. 11, p. 2799, 2022.

[14] Y. Cascone, V. Corrado, and V. Serra, "Calculation procedure of the shading factor under complex boundary conditions," *Solar Energy*, vol. 85, no. 10, pp. 2524–2539, 2011.

[15] S. Tazawa, "Effects of various radiant sources on plant growth (part 1)," *Japan Agricultural Research Quarterly*, vol. 33, pp. 163–176, 1999.

[16] J. Williams, C. Jones, J. Kiniry, and D. A. Spanel, "The EPIC crop growth model," *Transactions of the ASAE*, vol. 32, no. 2, pp. 497–0511, 1989.

[17] Heliene Inc. 132 Half-Cut Monocrystalline 515W – 535W. [Online]. Available: https://heliene.com/132hc-m10-tpc-sl-monofacial-module/

[18] REM TEC. Agrovoltaico. [Online]. Available: https://remtec.energy/en/agrovoltaico

[19] I. Reda and A. Andreas, "Solar position algorithm for solar radiation applications," *Solar energy*, vol. 76, no. 5, pp. 577–589, 2004.

[20] W. F. Holmgren, C. W. Hansen, and M. A. Mikofski, "pvlib python: A python package for modeling solar energy systems," *Journal of Open Source Software*, vol. 3, no. 29, p. 884, 2018.

[21] Gurobi optimizer 9.5.0. [Online]. Available: https://www.gurobi.com

[22] Daily agrivoltaic operation. [Online]. Available: https://github.com/astuhlmacher/DailyAgrivoltaicOperation